Multifunctional wet-white leather tanning system based on vegetable tannins and dual-functionalized zirconium phosphate nanoplatelets: Optimization, characterization, and applications

Jiabo Shi,[1, *] Yixuan Zeng,[1] Liyao Wang,[1] Miao Zhang,[2, *] Yi Zhang[3]

[1] College of Bioresources Chemical and Materials Engineering, Shaanxi University of Science & Technology, No.6 Xuefu Zhonglu, Weiyang District, Xi'an 710021, P. R. China

[2] School of Chemistry, Xi'an Jiaotong University, Xi'an 710049, P. R. China

[3] ISIS Neutron and Muon Source, Rutherford Appleton Laboratory, Didcot OX11 0QX, UK

ABSTRACT:

Tannic acid (TA), one of hydrolysable vegetable tannins, has been utilized to create wet-white tanning systems exhibiting enhanced synergistic effects with two-dimensional nanomaterials. Here, we present an effective strategy for structural stabilization of collagen fibers by dual-functionalized zirconium phosphate nanoplatelets (ZrP NPs) to achieve a TA based wet-white tanning system for the production of multifunctional eco-leather. By examining the influence of ZrP NPs and final pH value on tanning efficiency, we established a wet-white tanning system based on 10 wt.% TA and 3 wt.% ZrP NPs at final pH 3.5. Hydrogen-bonding and electrostatic interactions between the ZrP NPs and collagen fibers stabilized the collagen fibers, enabling hierarchical incorporations of ZrP NPs with the leather matrix. Moreover, we propose a mixed-dimensional materials design tactic enabled by polyphenol-mediated interface architecture to fabricate multifunctional wet-white leather-based triboelectric nanogenerator (TENGs) toward energy harvesting and flexible wearable electronics. The incorporation of α-zirconium phosphate nanoplatelets into the collagen fiber matrix with the aid of natural Tara tannins-mediated robust interfaces endows the TENGs with excellent mechanical properties, biodegradability, water vapor permeability, and flame retardancy. Furthermore, MXene ink is directly introduced into the collagen fiber matrix to enhance output charge density and sensing performance, enabling the TENGs to harvest ambient mechanical energy. Equally important, the as-prepared TENGs serve as self-powered flexible sensors for energy harvesting, human motion monitoring, and distress signaling. This work not only provides deeper insights into the design of multifunctional biomass-based TENGs but also highlights the critical role of multidimensional nanomaterial integration in advancing flexible electronics.

Keywords: eco-leather, triboelectric nanogenerators, zirconium phosphate nanoplatelets, dual-functionalization, polyphenol-mediated interface architecture

***Corresponding author:** E-mail: shijiabo@sust.edu.cn; miaozhangchem@xjtu.edu.cn

Introduction

The exploration of eco-friendly and sustainable tanning materials and associated tanning technologies has become a central focus in the leather-making, significantly contributing to sustainable development of leather industry. To replace traditional systems from the resource, various sustainable modification materials have been intensively developed.[1-4] Diverse modification systems by utilizing vegetable tannins have demonstrated particular promise as sustainable approaches for wet-white tanning systems, capitalizing on their natural origins and advantageous properties. Tannic acid (TA), one kind of hydrolysable vegetable tannins, has shown to create sustainable modification systems that exhibit enhanced synergistic effects with nanosilicates,[5] polymers,[6] and benzenesulphonate.[7] Our recent finding has demonstrated that two-dimensional zirconium phosphate nanoplatelets (ZrP NPs) can be potentially applied for the modification of collagen fibers (CF) matrix, conferring the leather matrix with multifunctional enhancements in ultraviolet barrier, antibacterial, and combustion suppression capabilities.[8]

Biomass-based materials have attracted immense attention for the creation of biodegradable TENGs owing to their intrinsic renewability, degradability, cost-effectiveness, and outstanding functional properties. The renewability and degradability of these materials also enable recycling and reusability, aligning with the principles of green chemistry. Among countless biomass-based materials, natural proteins, such as collagen, silk, and keratin, play a pivotal role in the fabrication of diverse TENGs.[9-11] Notably, Type I collagen fiber, primarily sourced from mammalian skin tissue, is an ideal biomass substrate for constructing new flexible sensors. Active functional groups within the collagen also make it an ideal choice for TENGs, and the unique hierarchical structure of collagen aids in the creation of sensing units in flexible and wearable sensors, thereby enhancing its sensitivity.[12-14] However, their implementation in practical devices is often impeded by insufficient mechanical strength, inadequate water vapor permeability (breathability), and poor flame retardancy. Therefore, it becomes imperative to explore high-performance protein-based TENGs with enriched functionalities.

In this work, we proposed an effective strategy for tailored structural stabilization of collagen fibers by dual-functionalized two-dimensional zirconium phosphate nanoplatelets (ZrP NPs) to optimize a tannic acid (TA) based wet-white tanning system towards multifunctional eco-leather manufacture. On the basis, we propose a mixed-dimensional materials design tactic enabled by polyphenol-mediated interface architecture to fabricate multifunctional collagen fiber-based TENGs toward energy harvesting and flexible wearable electronics.

Materials and methods

Materials. Pickled cattle hide was provided by Sichuan Dehua Leather Co., Ltd. (China). Tannic acid (TA) was purchased from the Institute of Chemical Industry of Nanjing Forest Products (China). Zirconium phosphate nanoplatelets (ZrP NPs) were bought from Chengdu Sunshine Factory Co., Ltd. (China). Tetrabutylammonium hydroxide (TBAOH), vinyl tri-methoxysilane (VTMS), 3-(aminopropyl) triethoxysilane (APTES), gallic acid (GA), 1-ethyl-3-(3-dimethylaminopropyl) carbodiimide (EDC) hydrochloride, acrylic acid (AA), and potassium persulfate (KPS) were from Tianjin Tianli Chemical Reagent Co., Ltd. (China), Ti_3AlC_2 and LiF were purchased from Shanghai Macklin Biochemical Technology Co., Ltd. (China). Silicone rubber was purchased from Smooth-On Company (USA). Other chemicals were obtained from Tianjin Tianli Chemical Reagent Co., Ltd. (China).

Methods. First, CF matrix treated with Tara tannins was immersed in 100% deionized water at 25°C, and 3% ZrP NPs were added for 2 h, with a final pH value adjusted at 3.5 using 1% formic acid. The resultant CF matrix (denoted as CTZ) was piled overnight, washed with 200% water, and dried at 60°C for 24 h. Then, a certain amount of MXene powder was added to deionized water and ultrasonically dispersed for 30 minutes to obtain a 10 $mg \cdot mL^{-1}$ MXene nanodispersion ink. The MXene nanodispersion ink was loaded into a spray bottle and evenly sprayed onto the grain side of the CTZ matrix. Finally, A 5 $mg \cdot mL^{-1}$ MXene dispersion was loaded into a commercially available air spray gun. The CTZ substrate was spray-coated with MXene through 2-3 coating cycles to ensure uniform surface coverage. Subsequently, the coated substrate was promptly transferred to a vacuum oven and dried at 50°C for 3 h to yield CTZM.

Results and discussion

The increase in shrinkage temperature (T_s) was a consequence of crosslinking within the collagen, which reflected the thermal resistance of fully water saturated leather, i.e. hydrothermal stability. Optimization of the TA-based tanning system revealed dual-functionalized ZrP-GA-AA NPs significantly enhance hydrothermal stability. While 10 wt% TA alone achieved a shrinkage temperature (T_s) of 60.2°C,[15] adding 3 wt% ZrP-GA-AA NPs increased T_s to 75.8°C surpassing values with pristine ZrP (63.2°C) or ZrP-GA (68.1°C) (Fig. 1a-b). This improvement stemed from synergistic crosslinking between TA and ZrP-GA-AA NPs. Hydrophilic GA and AA grafting facilitated the diffusion of ZrP NPs into the leather matrix (Fig. 1b inset), enhancing the binding efficiency of collagen.[16]

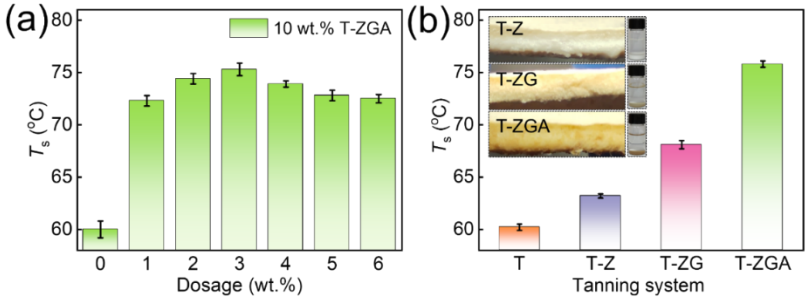

Fig. 1. (a) T_s of crust leathers tanned by the wet-white tanning system based on 10 wt.% TA combination with different dosage of ZrP-GA-AA NPs (T-ZGA). (b) T_s of crust leathers tanned by the wet-white tanning system based on solo 10 wt.% TA (T) and 10 wt.% TA combination with 3 wt.% pristine ZrP (T-Z), ZrP-GA (T-ZG), and ZrP-GA-AA NPs (T-ZGA), respectively. The inset shows the photographs of the penetration process of these ZrP NPs into the leathers along with the corresponding spent tan liquors during the tanning process.

Moreover, it was known that the enhancement of hydrothermal stability of the leather matrix was related to the filling and fixation of tanning materials by leathers.[17] Thickness measurements confirmed superior incorporation of dual-functionalized ZrP-GA-AA NPs versus pristine ZrP or ZrP-GA (Fig. 2a), facilitating hierarchical collagen integration.[18] pH optimization revealed peak performance at pH 3.5 (T_s = 75.8°C), close to isoelectric point of TA (3.5-4.0), where electrostatic deposition maximized. At pH 5.5, T_s dropped to 60.8°C (Fig. 2b). Therefore, 10 wt% TA combined with 3 wt% ZrP-GA-AA NPs at pH 3.5 was established as the optimal tanning system.

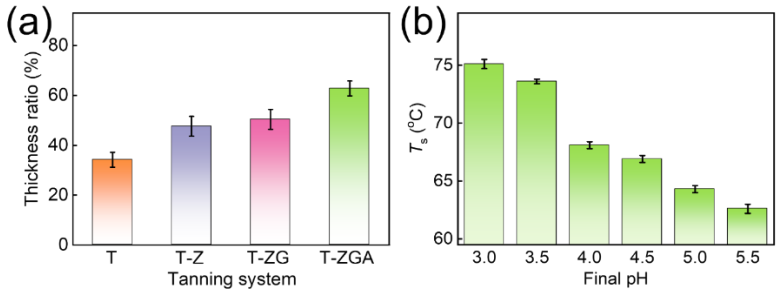

Fig 2. (a) The thickness ratio of crust leathers tanned by wet-white tanning system based on solo 10 wt.% TA (T) and 10 wt.% TA combination with 3 wt.% pristine ZrP (T-Z), ZrP-GA (T-ZG), and ZrP-GA-AA NPs (T-ZGA), respectively. (b) Final pH value dependence of T_s of the crust leathers tanned by 10 wt.% TA combined with 3 wt.% ZrP-GA-AA NPs.

It was recognized that Type I collagen was characterized by its hierarchical composition from different structural elements including molecules, microfibrils, fibrils, elementary fibers, fibers, and fiber networks. ATR-FTIR and WAXD analyses confirmed preservation of type I collagen's triple-helical structure across all modified leather matrices. Characteristic amide bands (Amide A and B at 3307 and 3064 cm^{-1}, I at 1648 cm^{-1}, II at 1550 cm^{-1}, III at 1240 cm^{-1}) remained unshifted post-modification. Structural integrity was evidenced by consistent Amide III/1450 cm^{-1} ratio (~1.0) and $\Delta\nu$(Amide I-II) less than 100 cm^{-1} (Fig. 3a). WAXD revealed homogeneous ZrP-GA-AA distribution (absent ZrP aggregation peak at 5.9°), with minor Peak I shifts indicating non-covalent collagen-NP interactions (hydrogen/electrostatic bonding) (Fig. 3b). This confirms dual-functionalized ZrP NPs maintain collagen microstructure while enabling uniform nanocomposite formation critical for mechanical performance.

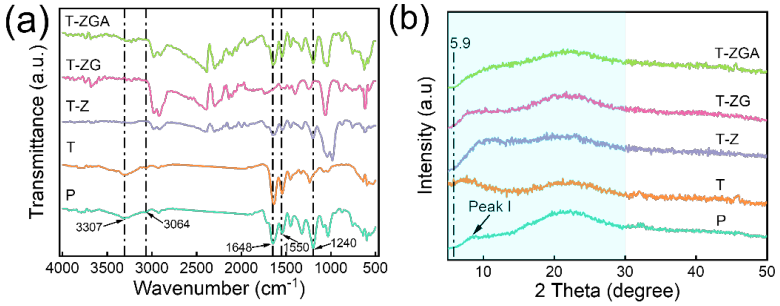

Fig 3. (a) ATR-FTIR spectra of Amide III (1240 cm^{-1}) to 1450 cm^{-1}, A_{III}/A_{1450}, and the difference between the wavenumbers of Amide I and II ($\Delta\upsilon$) of pristine CF (P) and wet-white leather matrices modified by solo TA (T), TA combined with pristine ZrP (T-Z), ZrP-GA (T-ZG), and ZrP-GA-AA NPs (T-ZGA). (b) WAXD of pristine CF (P) and wet-white leather matrices modified by solo TA (T), TA combined with pristine ZrP (T-Z), ZrP-GA (T-ZG), and ZrP-GA-AA NPs (T-ZGA).

The core challenge in the leather tanning systems lies in ensuring sufficient penetration and effective binding of nanomaterials in the collagen microstructures. SEM-EDS line scanning across the leather cross-section (Fig. 4a-c) confirmed simultaneous presence of collagen elements (C:44.8 wt%, N:7.2 wt%, O:21.3 wt%) and Zr (26.7 wt%) from ZrP-GA-AA NPs, verifying successful nanomaterial penetration. The decreasing Zr gradient from flesh to grain side (Fig. 4d) reflected histological variations in collagen fiber density, demonstrating microstructure-dependent nanoparticle distribution.

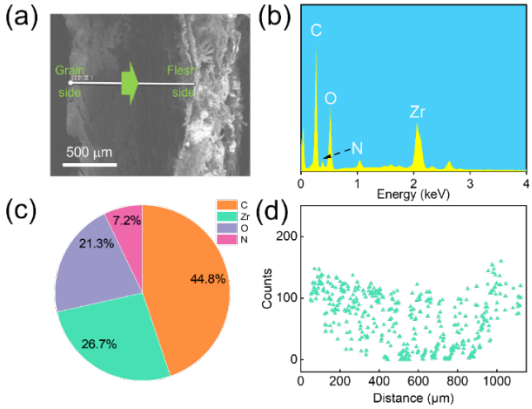

Fig 4. (a) FE-SEM image, (b) the corresponding EDX spectrum, (c) element compositions, and (d) EDS spectrum of cross section from the flesh side to grain side of the leather matrix.

The multiscale porous microstructures of collagen fibers provided suitable channels for the diffusion-penetration of two-dimensional nanomaterials, influencing the interfacial interactions with the collagen's hierarchical structures. FE-SEM revealed TA-induced collagen fiber bundling (Fig. 5a-c) with NPs (100–150 nm) bound on/between fibers. Further AFM confirmed preserved *D*-periodic banding in fibrils and NP dispersion at fibrillar interfaces (Fig. 5d), demonstrating hierarchical diffusion/fixation via collagen's porous network for structural stabilization (Fig. 5e).

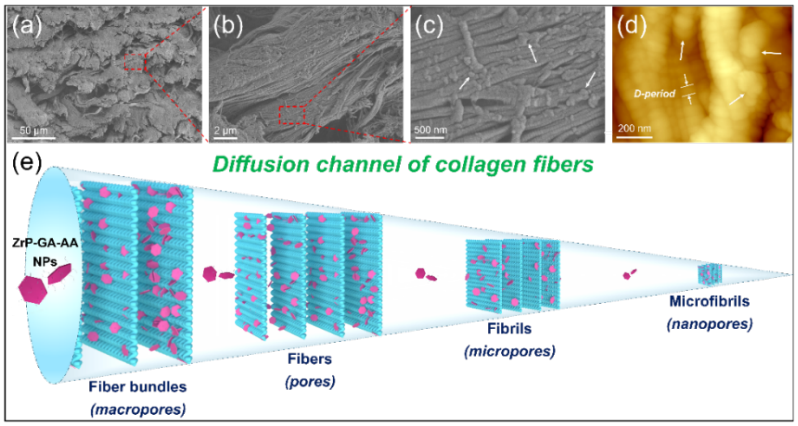

Fig 5. (a-c) FE-SEM images and (d) AFM image of wet-white leather matrix tanned by TA combined with ZrP-GA-AA NPs. (e) Schematic illustration showing the diffusion channel of collagen fibers.

Flexible, biodegradable, flame-retardant triboelectric nanogenerators (TENGs) were fabricated using polyphenol-mediated architecture. Goatskin collagen fiber matrix (C) was stabilized with Tara tannins (T) and zirconium phosphate nanoplatelets (Z), then coated with MXene nanosheets (M) as a triboelectric layer (termed as CTZM (Fig. 6a)). Cross-sectional FE-SEM confirmed robust adhesion of MXene nanosheets (M) to the CTZ matrix surface (Fig. 6b, c). Tara tannin (T) acted as a molecular bridge: forming hydrogen bonds with collagen fibrils (C) via amino/hydroxyl groups while crosslinking ZrP nanoplatelets (Z) through P-OH interactions and MXene (M) terminals via Ti-OH and Ti-F bonds (Fig. 6d). This hierarchical bonding network enhanced collagen matrix stability. EDX analysis verified successful integration of components: Zr (Z), Ti (M), and N/O (C) were uniformly distributed throughout CTZM (Fig. 6e,f), with elemental mappings confirming homogeneous dispersion of Z and M within the collagen matrix.

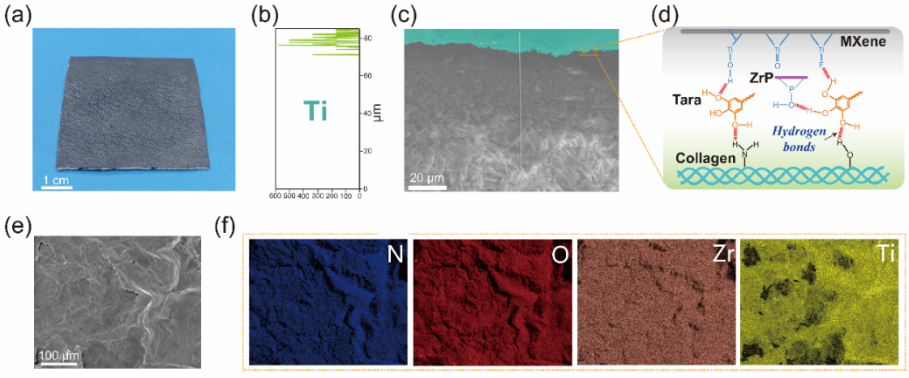

Fig. 6. Structure and properties of CTZM. (a) Digital photograph of the flexible CTZM film, (b) EDS spectrum of Ti, (c) cross-sectional FE-SEM image, and (d) schematic illustration showing interfacial interactions of CTZM. (e) Surface FE-SEM image and (f) EDX elemental mappings of N, O, Zr, and Ti

elements within CTZM. (g) SAXS and (h) enlarged profiles (intensity as a function of q), and SANS scattering patterns in (i) dried state and (j) hydrated state (soaked in D_2O) of C matrix, CT matrix, and CTZ matrix, respectively. (k) Tensile strength, (l) water vapor permeability, (m) heat release rate (HRR), and (n) total heat release (THR) of CT matrix and CTZ matrix.

We then investigated the influence of these building blocks on the microstructures of CTZ matrix. SAXS/SANS analysis revealed that incorporating Tara tannin (T) and ZrP nanoplatelets (Z) altered collagen matrix microstructures. While pure collagen (C) exhibited characteristic Bragg peaks corresponding to a 61.4 nm *D*-period, CT and CTZ matrices showed attenuated peaks (Fig. 7a,b). Intermolecular lateral packing distances (ILP) increased from 1.17 nm (C) to 1.30 nm (CT) and 1.22 nm (CTZ). CTZ uniquely displayed a broad peak at 0.24 $Å^{-1}$, suggesting ZrP colloidal aggregation. SANS confirmed a reduced *D*-period in D_2O-hydrated matrices (62.4 nm for CTZ vs. 63.5 nm for C) (Fig. 7c). Critically, an inverted $5^{th}/6^{th}$ peak intensity ratio indicated hydrogen bonding stabilizes collagen's triple helix in CTZ, enhancing flexibility (Fig. 7d).

We further investigated the influence of building blocks on the mechanical properties of the CTZ matrix. Mechanical testing revealed synergistic reinforcement: Incorporating ZrP nanoplatelets (Z) with Tara tannin-modified collagen (CT) increased tensile strength from 21.9 MPa (CT) to 23.9 MPa (CTZ) and strain at break from 95.9% to 108.7% (Fig. 7e). This enhancement was attributed to increased collagen crosslinking. Moreover, compared to the CT matrix, the resulting CTZ matrix presents enhanced water vapor permeability from 4888.2 to 7562.7 $mg·(cm^2·h)^{-1}$ (Fig. 7(f)), indicating that incorporating functional T and Z building blocks with collagen significantly enhanced the breathability of the CTZ matrix.Cone calorimetry confirmed ZrP (Z) significantly enhanced flame retardancy: CTZ exhibited a 22.8% reduction in peak heat release rate (pHRR: 185.2 vs. 239.9 $kW·m^{-2}$) and 28.7% lower total heat release (THR: 9.7 vs. 13.6 $MJ·kg^{-1}$) versus CT (Fig. 7g,h). This improvement stemmed from ZrP-induced char formation—which created a dense carbon layer that blocked heat/gas transmission during combustion. Crosslinking by ZrP further densified the protective char. Comparative analysis demonstrated CTZ's superior flame suppression over benchmark systems, evidenced by markedly lower pHRR.

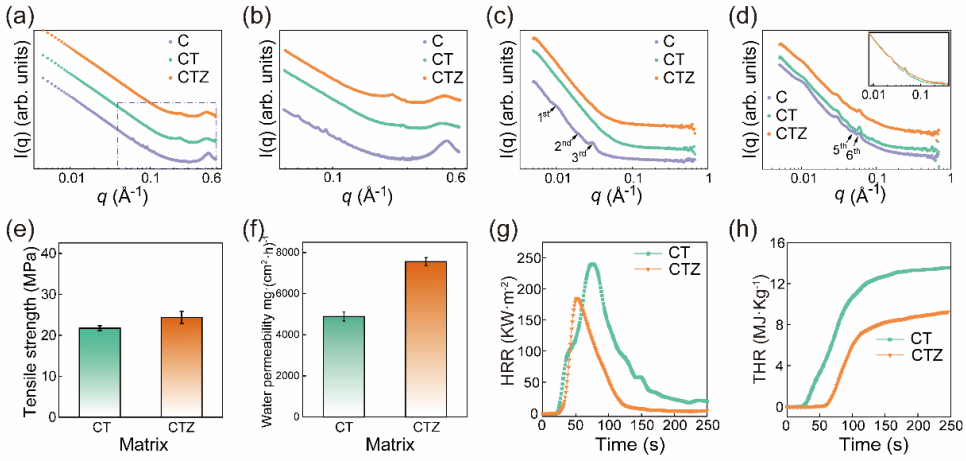

Fig. 7. (a) SAXS and (b) enlarged profiles (intensity as a function of q), and SANS scattering patterns in (c) dried state and (d) hydrated state (soaked in D_2O) of C matrix, CT matrix, and CTZ matrix, respectively. (e) Tensile strength, (f) water vapor permeability, (g) heat release rate (HRR), and (h) total heat release (THR) of CT matrix and CTZ matrix.

TENG-1 demonstrated real-time motion sensing on human joints, generating higher voltages at the elbow (~30 V) versus fingers (~16 V) due to greater movement amplitude (Fig. 8a-d). TENG-3 functioned as a handwriting sensor, producing distinctive voltage peaks corresponding to pen pressure during writing (e.g., TENG, MXene, Leather in Fig. 8e-h). Unique signal patterns enabled letter differentiation, confirming CTZM's repeatability, sensitivity, and identifiability as a self-powered sensor.

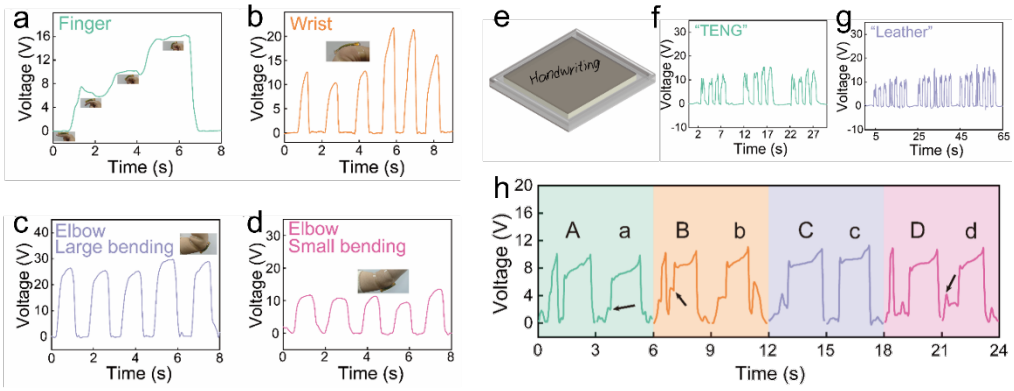

Fig. 8. (a) Voltage signals of TENG-1 in response to the finger bends in 30°, 60°, and 90°. Voltage signals of TENG-1 in response to the bends of (b) wrist, (c) elbow with large bending, and (d) elbow with small bending. (e) Schematic illustration of TENG-3. (f-h) Repeatable voltage signals for sensing different handwriting details.

Fig. 9a-b illustrated a schematic diagram of CTZM-TENGs harvesting mechanical energy from human motion. CTZM-TENGs harvested biomechanical energy from body movement, with rectified output powering electronics: TENG-2 charged a 4.7 μF capacitor to illuminate an LED (Fig. 9c(i)), while larger TENG-3 sustained a temperature/humidity meter (Fig. 9c(ii)). An insole-shaped TENG-4 activated dozens of LEDs during walking (Fig. 9c(iii)). Resistance-dependent testing revealed a peak power density of 234.63 $mW \cdot m^{-2}$ at 250 MΩ for TENG-3 (Fig. 9d-e), demonstrating efficient energy conversion. Fig. 9f demonstrated the capacitive charging capability of TENG-3 using capacitors with different capacitances (4.7 μF, 10 μF, 47 μF, and 100 μF). Under 20 seconds of operational time, the voltages across these capacitors attained 5.80 V, 3.14 V, 0.96 V, and 0.52 V, respectively.

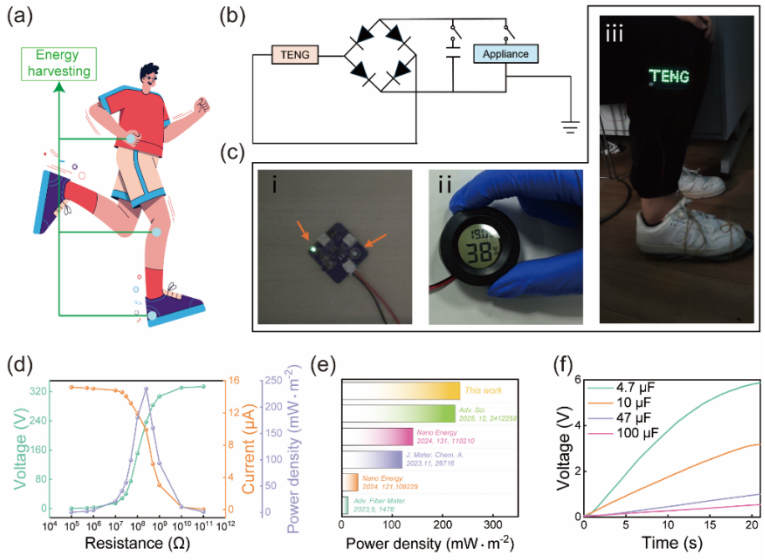

Fig. 9. (a) Schematic diagram showing the CTZM-TENGs for harvesting human energy.(b) Schematic circuit diagram of TENG for powering application. (c) Digital photos of the CTZM-TENGs powering various electrical devices. (d) Output voltage, output current and power density of TENG-3 with different external load resistances. (e) Comparisons of power density between the CTZM-TENG and previously reported flame-retardant TENGs. (f) Charging curves of different capacitors ranging from 4.7 μF to 100 μF.

Based on the excellent flame retardancy and electrical properties of CTZM-TENG above, we also developed a self-powered distress signaling system with autonomous alarm functionality comprising the TENG unit, DSP processor, Bluetooth module, and smartphone app. Upon mechanical pressure, signals were processed and wirelessly transmitted as Morse code alerts. The TENG functioned as a portable/installable emergency device (Fig. 10a), enabling trapped individuals in fires to trigger frequency-specific distress signals for rescue teams (Fig. 10b). This integrated system demonstrated self-powering capability, rapid response, and modular intelligence for fire-safe wearable electronics in emergency scenarios.

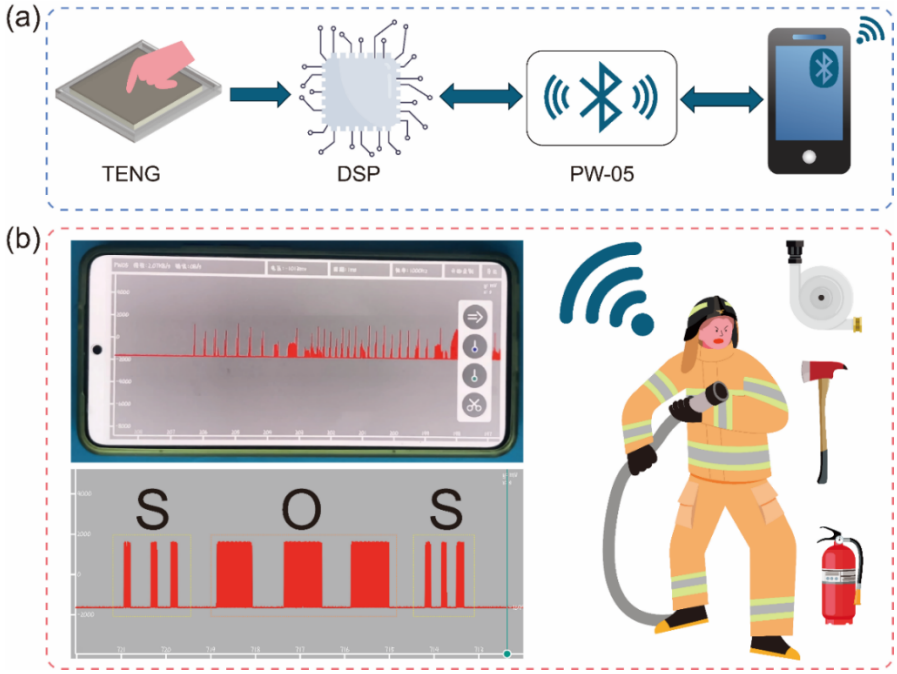

Fig. 10. (a) Schematic of the fire-alarm system based on TENG; TENG-based fire alarm system: (b) Mobile App interface and application scenarios.

Conclusions

In summary, we developed dual-functionalized ZrP NPs (GA/AA-grafted) for collagen stabilization in eco-leather and TENGs. Optimized tanning used 10 wt% TA combined with 3 wt% ZrP-GA-AA at pH 3.5, where H-bonding/electrostatic interactions preserved collagen microstructure (ATR-FTIR/WAXD) and enabled hierarchical NP integration (FE-SEM/AFM) without disrupting *D*-periodicity. Simultaneously, flexible collagen-based TENGs were fabricated via polyphenol-mediated architecture: Tara tannins bridged ZrP nanoplatelets within the matrix, endowing biodegradability, flame retardancy, and breathability. MXene coating enhanced charge density, enabling self-powered sensors for motion/handwriting detection and biomechanical energy harvesting.

Acknowledgements

The authors acknowledge the financial support from the National Natural Science Foundation (NNSF) of China (22208201), the China Postdoctoral Science Foundation (2023M743106), the Sichuan Science and Technology Program (2024ZHCG0082), and the Central Guidance Fund for Local Scientific and Technological Development Projects (2023ZYDF037).

References

[1] W. Ding, X. Pang, Z. Ding, D.C.W. Tsang, Z. Jiang, B. Shi, Constructing a Robust Chrome-Free Leather Tanned by Biomass-Derived Polyaldehyde via Crosslinking with Chitosan Derivatives, Journal of Hazardous Materials 396 (2020) 122771.

[2] Q. Luo, C. Li, W. Zhao, W. Ding, Y. Liu, W. Xiao, H. Liu, X. Pang, J. Sun, Lignin Demethylated by Protic Ionic Liquid as a Novel and Sustainable Chrome-Free Tanning Agent for Eco-Leather Production, ACS Sustainable Chemistry & Engineering 12(26) (2024) 9682-9694.

[3] X. Dang, H. Qiu, S. Qu, S. Liang, L. Feng, X. Wang, β-Cyclodextrin-Based Chrome-Free Tanning Agent Results in the Sustainable and Cleaner Production of Eco-Leather, ACS Sustainable Chemistry & Engineering 12(9) (2024) 3715-3725.

[4] Y. Yu, H. Wang, Y. Zeng, J. Zhou, Y. Zhang, B. Shi, Y.-n. Wang, Biomass-Derived Polycarboxylate–Aluminum–Zirconium Complex Tanning System: A Sustainable and Practical Approach for Chrome-Free Eco-Leather Manufacturing, Journal of Cleaner Production 452 (2024) 142261.

[5] J. Shi, R. Zhang, Z. Mi, S. Lyu, J. Ma, Engineering a Sustainable Chrome-Free Leather Processing Based on Novel Lightfast Wet-White Tanning System towards Eco-Leather Manufacture, Journal of Cleaner Production 282 (2021) 124504.

[6] X. Pan, R. Li, W. Li, W. Sun, Y. Yan, X. Xiang, J. Fang, Y. Liao, C. Xie, X. Wang, Y. Cai, X. Yao, H. Ouyang, Silk Fibroin Hydrogel Adhesive Enables Sealed-Tight Reconstruction of Meniscus Tears, Nature Communications 15(1) (2024) 2651.

[7] Y.H. Xiao, C.H. Wang, J. Sang, W. Lin, A Novel Non-Pickling Combination Tanning for Chrome-free Leather Based on Reactive Benzenesulphonate and Tannic Acid, Journal of the American Leather Chemists Association 115(1) (2020) 16-22.

[8] J. Shi, Y. Zhang, N. Yang, X. Guan, L. Sheng, L. Liu, W. Zhong, Covalently Surface-Grafting A-Zirconium Phosphate Nanoplatelets Enables Collagen Fiber Matrix with Ultraviolet Barrier, Antibacterial, and Flame-Retardant Properties, International Journal of Biological Macromolecules 254 (2024) 127999.

[9] C.M. Jiang, Q. Zhang, C.X. He, C. Zhang, X.H. Feng, X.J. Li, Q. Zhao, Y.B. Ying, J.F. Ping, Plant-Protein-Enabled Biodegradable Triboelectric Nanogenerator for Sustainable Agriculture, Fundamental Research 2(6) (2022) 974-984.

[10] N.R. Kheirabadi, F. Karimzadeh, M.H. Enayati, E.N. Kalali, Green Flexible Triboelectric Nanogenerators Based on Edible Proteins for Electrophoretic Deposition, Advanced Electronic Materials 9(2) (2023).

[11] F.G. Torres, K.N. Gonzales, O.P. Troncoso, J.I. Corman-Hijar, G. Cornejo, A Review on the Development of Biopolymer Nanocomposite-Based Triboelectric Nanogenerators (Bio-TENGs), ACS Applied Electronic Materials 5(7) (2023) 3546-3559.

[12] L.Y. Li, J. Zhang, M.T. Wang, J.Q. Zhang, X.F. Zeng, J.X. Wang, Y. Le, Electrospun Hydrolyzed Collagen from Tanned Leather Shavings for Bio-Triboelectric Nanogenerators, Materials Advances 3(12) (2022) 5080-5086.

[13] O.Y. Yue, X.C. Wang, Y. Zhou, Z.X. Bai, X.L. Zou, L. Xie, X.H. Liu, Auxetic Structure-Assisted Triboelectric Nanogenerators for Efficient Energy Collection and Wearable Sensing, Advanced Energy Materials 14(24) (2024).
[14] O. Yue, X. Wang, M. Hou, M. Zheng, Z. Bai, B. Cui, S. Cha, X. Liu, Skin-Inspired Wearable Self-Powered Electronic Skin with Tunable Sensitivity for Real-Time Monitoring of Sleep Quality, Nano Energy 91 (2022) 106682.
[15] F.H. Heijmen, J.S. duPont, E. Middelkoop, R.W. Kreis, M.J. Hoekstra, Cross-Linking of Dermal Sheep Collagen with Tannic Acid, Biomaterials 18(10) (1997) 749-754.
[16] J.M. Morera, E. Bartolí, B. Esteban, Study of the Hydrothermal Stability of Leather Tanned with Vegetable Extracts Using an Isometric Method, Thermochimica Acta 742 (2024) 179893.
[17] X.R. Guo, Y. Yu, Y.N. Wang, B. Shi, Oxidized Maltodextrin: A Novel Ligand for Aluminum-Zirconium Complex Tanning, Journal of the American Leather Chemists Association 116(5) (2021) 155-161.
[18] J. Shi, C. Wang, T. Ngai, W. Lin, Diffusion and Binding of Laponite Clay Nanoparticles into Collagen Fibers for the Formation of Leather Matrix, Langmuir 34(25) (2018) 7379-7385.